Applied Surface Science 684 (2025) 161927

Contents lists available at ScienceDirect

Applied Surface Science

journal homepage: www.elsevier.com/locate/apsusc

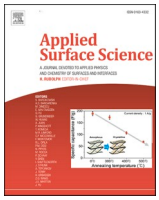

Full Length Article

Dioctyl sulfosuccinate sodium salt (AOT) as a corrosion inhibitor for AZ31 Mg alloy: Effects of integration with layered double hydroxide (LDH)

Roya Malekkhouyan [a], Yoann Paint [b], Xavier Noirfalise [b], Maurice Gonon [a], David Cornil [c], Jérôme Cornil [c], Marie-Georges Olivier [a,b,*]

[a] Materials Science Department, University of Mons, Place Du Parc 20, Mons 7000, Belgium
[b] Materia Nova Research Center, Parc Initialis, 7000 Mons, Belgium
[c] Laboratory for Chemistry of Novel Materials, University of Mons, Place Du Parc 20, Mons 7000, Belgium

ARTICLE INFO

Keywords:
Dioctyl sulfosuccinate sodium salt
AOT
AZ31 magnesium alloy
Corrosion inhibitor
Corrosion resistance
Conversion coating
Layered double hydroxide
LDH

ABSTRACT

Surfactants are known for their corrosion inhibition effect for metallic substrates like magnesium (Mg) alloys. Among these surfactants, dioctyl sulfosuccinate sodium salt, also known as AOT, is noteworthy. The present study investigates the corrosion inhibition of AOT on AZ31 Mg alloy using electrochemical impedance spectroscopy (EIS). In addition, surface characterization is conducted through scanning electron microscopy (SEM), energy-dispersive X-ray spectroscopy (EDS), X-ray diffraction (XRD), and X-ray photoelectron spectroscopy (XPS). Moreover, the interaction energy between AOT and the substrate is determined using Density Functional Theory (DFT) calculations. It is observed that AOT is effective for corrosion inhibition by being adsorbed on the surface of Mg alloy. The DFT calculations yield −5.25 eV value as interaction energy confirming the EIS results and the ability of AOT to prevent corrosion. The other part of this study involves incorporating AOT in layered double hydroxide (LDH) and demonstrating the enhanced corrosion resistance of the conversion layer facilitated by the surfactant. The existence of LDH structure after immersion in AOT solution was confirmed by SEM images and XRD test. The LDH structure was enhanced by increasing LDH inner layer thickness (from 11.8 ± 0.2 μm in LDH to 16.3 ± 0.3 μm) due to the addition of AOT, resulting in improved corrosion resistance of the substrate. These findings have significant implications for utilizing AOT as a corrosion inhibitor, particularly in the context of organic coatings, where AOT can serve as a vital link between the substrate and the organic coating.

1. Introduction

The standard potential of magnesium (Mg) is −2.37 V, making it prone to forming an oxide layer [1]. However, this oxide layer is not as effective in providing protection compared to metals such as aluminum or iron. For this reason, enhancing corrosion resistance in Mg alloys is crucial for their practical use in industry [2–4]. In order to achieve this, surface treatments can be employed to delay the contact between the corrosive media and the substrate [5]. These techniques have attracted attention due to their simplicity and cost-effectiveness [6,7]. Layered double hydroxide (LDH) represents a type of conversion coating that can be formed directly on the surface of substrates [8–10] or produced beforehand and subsequently applied to the surface [11,12]. LDH belongs to the class of nanosheets, which are composed of metal cations (both di- and trivalent) and interlayer anions that balance the charges [13–16]. These interlayer anions are exchangeable and can be replaced by the corrosive anions present in the media. Furthermore, if the released interlayer anion functions as a corrosion inhibitor, it can further enhance the corrosion resistance [17]. Corrosion inhibitors are chemical compounds utilized to delay or prevent the corrosion of metals [18]. They regulate the corrosion behavior in corrosive media when adsorbed onto the metal surface and forming a protective film [19,20].

Surfactants at low concentrations can also function as corrosion inhibitors by adsorbing onto substrate surfaces and reducing interfacial free energies. These surfactants consist of a long hydrocarbon chain and an ionic head [21]. Their superior inhibitory properties, environmentally friendly nature, and cost-effectiveness make them well-suited for industrial applications [22,23]. Anionic surfactants (surfactants with a negatively charged head) have demonstrated significant corrosion inhibition by forming a protective barrier layer on the metallic substrate and preventing species transfer from the electrolyte to the surface [24]. The corrosion inhibition efficiency of surfactants is influenced by several factors, including the length of the tail, electronegativity of the head, and solubility in aqueous media [22]. Research has demonstrated that

* Corresponding author.

https://doi.org/10.1016/j.apsusc.2024.161927
Received 27 September 2024; Received in revised form 21 November 2024; Accepted 24 November 2024
Available online 27 November 2024

increasing the chain length up to a certain point can enhance corrosion inhibition [25]. Furthermore, the length of the chain can impact the electronegativity of the head and subsequently the adsorption of the surfactant on the substrate. Additionally, the solubility of surfactants in aqueous media is restricted by the long tail [22]. The adsorption of surfactants plays a crucial role in determining hydrophobicity and corrosion protection. It is influenced by various factors such as covalent bonding, electrostatic attraction, hydrogen bonding, non-polar interactions between the adsorbed species, solvation, and desolvation [26]. These parameters are governed by the properties of the surfactant head and hydrophobic tail, functional groups of the surfactants, the substrate in contact with the solution, and the conditions of the solution in which the sample is immersed (e.g., pH, electrolyte concentration, polarity, temperature, etc.) [20]. The adsorption of corrosion inhibitors (and/or surfactants) onto the substrate can be investigated using Langmuir adsorption isotherms [23] or by calculating the adsorption energy using density functional theory (DFT) [27].

Different surfactants were utilized to inhibit the corrosion of Mg alloys. For instance, Frignani et al. [28] employed sodium salts of lauryl sulphate, N-lauroylsarcosine, N-lauroyl-N-methyltaurine, and dodecylbenzenesulfonic acid. Among these, dodecylbenzensulphonic acid exhibited the most effective inhibition due to its rapid adsorption and the formation of a thick and protective layer when combined with Mg cations. Additionally, the corrosion inhibition properties of sodium dodecyl sulphate (SDS) and sodium dodecylbenzenesulfonate (SDBS) for Mg alloys have been reported due to the presence of lone pair electrons in sulfur and oxygen, as well as the benzene ring in SDBS [23,27,29,30]. Lu et al. [23] investigated the corrosion inhibition mechanism of SDS on AZ91 Mg, which involves chemisorption of SDS on cathodic zones (intermetallic) and physisorption on corrosion products that suppress cathodic and anodic corrosion, respectively. The hydrophobic tail of SDS can increase the contact angle of water by forming a protective layer on the surface [27]. Dioctylsulfosuccinate Sodium (AOT – Aerosol OT) is an anionic surfactant with the chemical formula $C_{20}H_{37}NaO_7S$. AOT has low toxicity, is environmentally acceptable, and has a low cost, making it suitable for corrosion inhibition applications [31,32]. Its utilization as an anionic surfactant in an acidic environment has demonstrated corrosion inhibition for mild steel and AZ91 Mg alloy substrates [33,34].

The combination of LDH with surfactants can be employed to enhance and modify the corrosion protection of coatings for longer immersion periods. Previous research utilized sodium laurate [35], aspartic acid [36], lauric acid [37], and SDS [29] with LDH using anion exchange and one-pot intercalation methods. In this study, the corrosion of AZ31 Mg alloy was evaluated in the presence of a new anionic surfactant (AOT) with long hydrocarbon chains and ester groups by conducting electrochemical investigations and DFT calculations. Furthermore, the physical and chemical effects of AOT on the surfaces of Mg alloy and LDH were investigated, revealing the corrosion inhibition capability of AOT and enhanced corrosion resistance of LDH coatings with the application of AOT.

2. Experimental procedures

2.1. Materials

AZ31 Mg alloy sheets with a composition of 2.5–3.5 % Al, 0.7–1.3 % Zn, 0.2 % Mn, 0.05 % Si, 0.05 % Cu, 0.04 % Ca, 0.005 % Fe, 0.1 % Ni (wt %) and balance Mg (supplied from KG Fridman AB (SWEDEN)) was used for the substrate. Ammonium nitrate (NH_4NO_3) and AOT were purchased from RPL and Thermoscientific, respectively. Sodium chloride (NaCl) (EMSURE product line), aluminum nitrate nonahydrate ($Al(NO_3)_3{\cdot}9H_2O$), and sodium hydroxide (NaOH) (EMPLURA product line) were obtained from Sigma-Aldrich. Nitric acid (HNO_3) was acquired from VWR.

2.2. Preparation of substrates

All samples with dimensions 50 mm × 37 mm × 1 mm were pretreated with nitric acid prior to utilization. Initially, the samples were immersed in a solution of 2 M HNO_3 for a duration of 30 s, followed by rinsing with deionized water and subsequent immersion in a 0.25 M HNO_3 solution. The samples were rinsed once again with water and dried using a stream of air [38,39].

2.3. Preparation of solutions containing surfactant

0.1 M NaCl solution was used for EIS and immersion tests. The solubility of AOT in water at 25 °C is 1.5 g in 100 mL water; however, the existence of NaCl can decrease critical micelle creation [40]. To avoid the creation of micelles in the presence of 0.1 M NaCl solution, 0.45 mM AOT solution was produced (this solution is called NaCl + AOT solution). This solution was used to investigate the corrosion inhibition efficiency of AOT on AZ31 Mg alloy.

2.4. LDH formation and modification

Acid-pretreated surfaces of Mg alloys were used for the formation of LDH. To accomplish this, a solution containing 0.6 M NH_4NO_3 and 0.1 M $Al(NO_3)_3$ with pH of 11 (using 2 M NaOH solution) was prepared. This solution along with the etched surfaces of Mg alloys were placed in Teflon-lined autoclaves and were heated to 125 °C for 24 h [38,39].

After the formation of LDH on the surface of substrates, a 0.1 M saturated solution of AOT was used to modify the LDH coatings. The substrates coated with LDH were immersed in the AOT solution for 18 h at 60 °C.

3. Characterization

The electrochemical impedance spectroscopy (EIS) was performed in 0.1 M NaCl solution, and NaCl + AOT solution using a ModulLab controlled by XM-Studio® software. A classical three-electrode system, which consisted of a platinum counter electrode, an Ag/AgCl (sat. KCl) reference electrode, and samples, as working electrodes with an exposed area of 1 cm^2 were used. EIS measurements were performed in a frequency range from 100 kHz to 100 mHz with 61 points using a 10 mV peak-to-peak sinusoidal voltage. Moreover, pH measurements were performed at different immersion times in 0.1 M NaCl and NaCl + AOT solutions. For this purpose, substrates with dimensions of 2 cm × 2 cm × 1 mm (two sides) were in contact with 15 mL of each solution. A hydrogen (H_2) evolution setup was employed to further investigate corrosion resistance. H_2 evolution test was conducted (at least twice to confirm the reproducibility of the results) to examine the effect of AOT on the corrosion inhibition of both bare substrates (NaCl and NaCl + AOT) and those coated with the LDH layer (LDH and LDH + AOT). The sample dimensions were 40 mm × 40 mm × 1 mm for the bare substrates and 37 mm × 37 mm × 1 mm for the LDH-coated substrates, with a solution volume of 500 mL in the setup. The inhibition efficiency (IE) of AOT is determined using Equation (1), where V_{NaCl} and $V_{NaCl+AOT}$ represent the volumes of hydrogen evolved upon immersing the bare substrates in the NaCl solution without and with the addition of the inhibitor (AOT), respectively.

$$IE = [(V_{NaCl} - V_{NaCl+AOT})/V_{NaCl}] \times 100 \quad (1)$$

The surface morphologies, and thickness of layers, as well as the elemental composition of samples were investigated by scanning electron microscope (SEM, Hitachi SU8020) equipped with an energy dispersive X-ray spectrometer analyzer (EDS, Thermo Scientific Noran System 7). To obtain cross-section images, samples were embedded in resin (EpoFix resin and EpoFix hardener) and Struer TegraForce-5 was used for grounding them with 800, 1200, 2000, and 4000 SiC papers.

The crystalline structure of surfaces was investigated with X-ray diffraction (XRD, Panalytical Empyrean Theta – Theta) with CuKα radiation (λ = 0.154056 nm) and Ni filter with a step of 0.02° and a scanning rate of 1.2°/min in the 2θ range from 4° to 70°. A PHI Genesis apparatus was utilized for XPS measurements to analyze the chemical composition. A monochromatized Al Ka line (1486.6 eV) was operated as an incident photon source for XPS characterization. Photoelectron spectrum was accumulated at the take-off angle of 90° with respect to the surface normal. The XPS survey was acquired using a pass energy of 224 eV with a 0.4 eV step. The high-resolution spectra were acquired with a pass energy of 27 eV with a 0.2 eV step. All spectra were charge-corrected regarding the hydrocarbon constituent of the C1s peak at 285 eV.

The contact angle of the water droplet on the surface of samples were measured using DIGIDROP (IME-UDH-009) equipped with a digital camera and Visiodrop software. Water droplets with a volume of 1 μL were dispensed on the surfaces.

The interaction between the AOT surfactant and magnesium surface was further described by quantum-chemical calculations. AZ31 Mg alloy contains about 95–96 % of Mg in total composition; therefore, its surface was described with the 4-layers Mg surface used in our previous work [39]. All calculations were done at the Density Functional Theory (DFT) level with a periodical slab approach using the 6.2 version of VASP (Vienna Ab Initio Simulation Package) [41,42]. The PAW scheme (projected augmented wave) was used with a plane-wave basis set of 500 eV. The exchange-–correlation was treated with the PBE functional [43] and van der Waals interactions described with the DFT-D3 grimme approach [44,45]. The AOT molecule and the two top layers of the Mg surface were allowed to relax during the geometry optimization process. We used the conjugated gradient algorithm with an atomic force criterion of 0.01 eV/ Å.

The optimized salt structure consists of the AOT adsorbed on the surface and the sodium ion (Na^+) also present in the unit cell to conserve a charge neutrality. Therefore, the interaction energy, E_{int}, was calculated (using Equation (2)) as the difference between the total energy of the relaxed interface ($E_{AOT+Na/Mg}$) and the energy of the AOT only (E_{AOT}) and surface with the sodium (E_{Mg+Na}), in their relaxed interfacial geometry.

$$E_{int} = E_{AOT+Na/Mg} - [E_{Mg+Na} + E_{AOT}] \quad (2)$$

The atomic charges and bond orders intensities were computed using the DDEC/6 partition scheme [46].

4. Results and discussion

4.1. Corrosion inhibition of AOT on bare AZ31

4.1.1. Electrochemical investigations

To study the effect of AOT on the corrosion behavior of AZ31 Mg alloy, EIS tests were performed at different immersion times, as shown in Fig. 1. The value of impedance modulus at low frequency can be considered as the corrosion resistance of the whole system [38]. Fig. 2(a) presents a more accurate depiction of the impedances at the frequency of 0.1 Hz. Following a 24-hour immersion period in NaCl + AOT solution, the impedance modulus increased to 1.5 × 10^3 ohm.cm^2, which is 4 times higher than the impedance observed for Mg alloy immersed in NaCl solution for the same duration. These findings demonstrate the improved corrosion resistance of the substrates over time and the

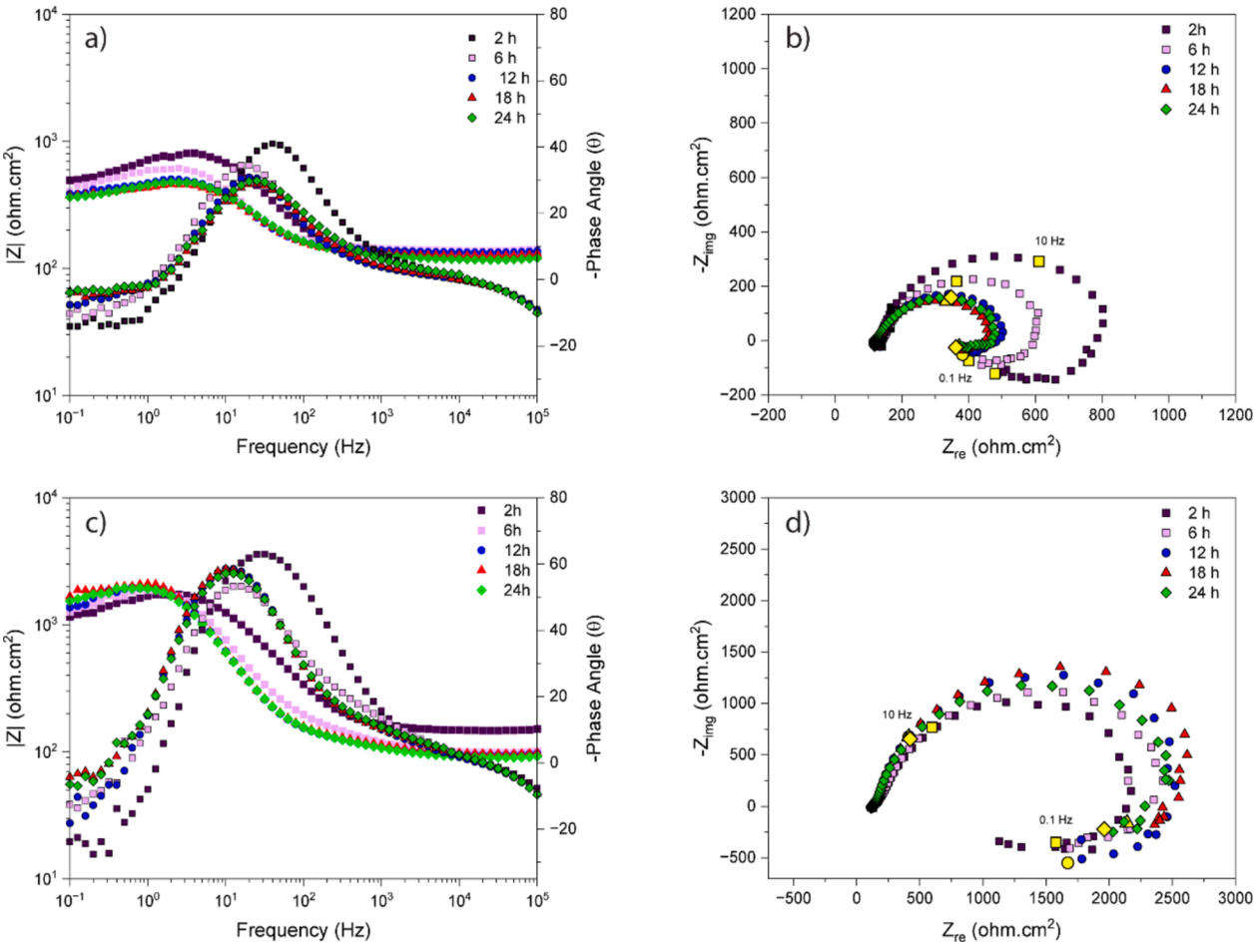

Fig. 1. Bode and Nyquist plots of AZ31 Mg alloy exposed to a), b) NaCl, and c), d) NaCl + AOT solutions.

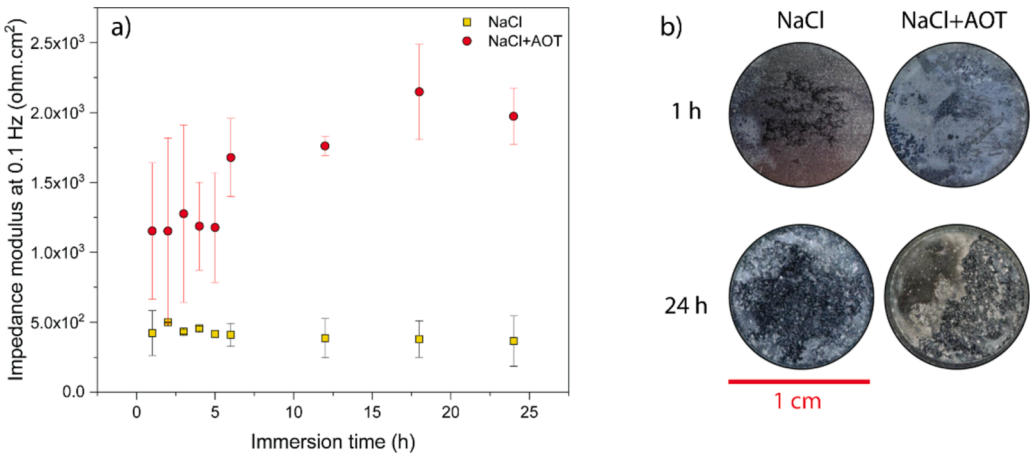

Fig. 2. a) Evolution of impedance modulus at low frequency for samples at different immersion times, and b) macroscopic images of sample surfaces after 1 h and 24 h.

capacity of AOT to hinder and reduce the corrosion rate. The slight elevation in impedance at low frequency after 24 h for the NaCl solution can be attributed to the formation of a thin oxide layer on the surface [47].

The inductive behavior of AZ31 in NaCl solution can be due to the non-stationarity of Mg substrate that can cause polarization of the Mg surface [48]; however, when AOT is present in the solution, the inductive loop is smaller. Surfactants have the ability to reduce the surface energy [21], and in the case of immersion in NaCl + AOT solution, it can be concluded that the surface is more stable, thereby decreasing the occurrence of inductive behavior. The Bode phase diagram of AZ31 in NaCl solution exhibits a peak at a frequency range of 10–10^3 Hz, which is associated with the formation of an oxide film on the substrate surface [47]. When the sample is immersed in NaCl + AOT solution, the Bode phase and Nyquist diagrams reveal the presence of a capacitive loop with passing time. This capacitive loop expands to more negative values

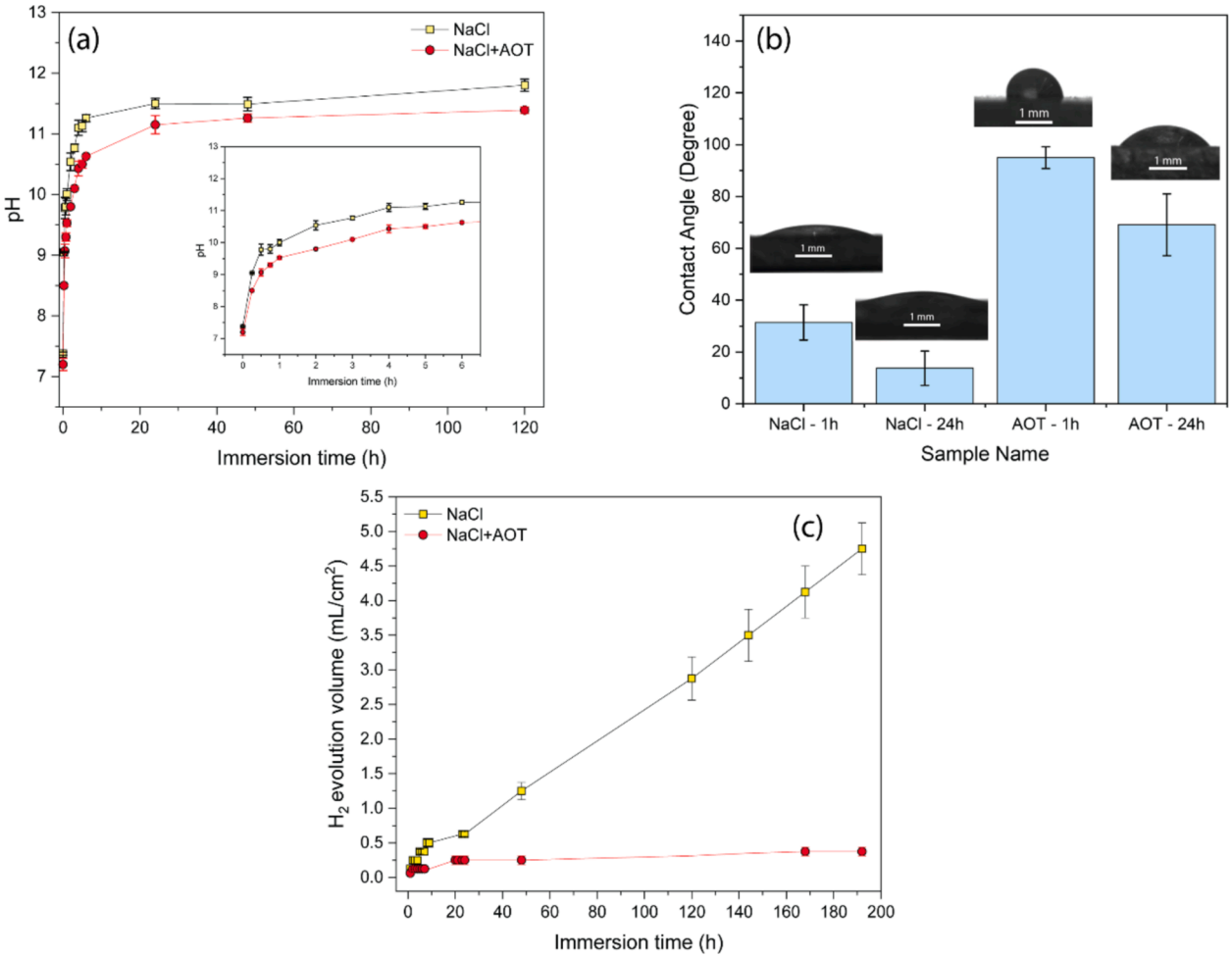

Fig. 3. Evolution of a) pH, b) contact angle, and c) hydrogen evolution volume, of samples during different immersion times.

of the phase angle, indicating the formation and growth of a surface film [47].

Fig. 2(b) shows the macroscopic images of samples after EIS tests after 1 h and 24 h. The formation of a white film on the surface of the substrate can be observed after 1 h immersion in NaCl + AOT solution. Moreover, after 24 h immersion in NaCl + AOT solution, along with the formation of a white layer, a smaller surface area was corroded in comparison to the sample in NaCl solution.

4.1.2. Immersion test, pH measurements, and H_2 evolution test

The corrosion reaction of Mg is accompanied by the increase in the pH of the solution due to the production of OH^- according to Reaction (1) [49,50].

$$Mg + 2H_2O \rightarrow Mg^{2+} + 2OH^- + H_2 \quad (1)$$

The pH measurements were performed for AZ31 substrates immersed in NaCl and NaCl + AOT solutions for 5 days. Analysis of the graphs depicting samples reveals that immersion in NaCl solution causes the pH to reach around 11.8 after 5 days of immersion. In the presence of AOT in the solution, the pH reaches a value of 11. Furthermore, it is observed that the rate at which the pH increases during the initial 6 h of immersion (as depicted in Fig. 3(a)) is lower in the case of AOT compared to the NaCl solution showing the corrosion inhibition ability of this compound.

Immersion of AZ31 in NaCl + AOT solution after 1 h increased the contact angle of water on the surface to 95° ± 4 in comparison to immersion in NaCl solution (31° ± 6). It can be inferred that AOT is adsorbed on AZ31 through the S group head and the presence of the alkyl chain on the surface may enhance the surface hydrophobicity. This could explain the observed increase in contact angle after immersion in the NaCl + AOT solution for 1 h. After 24 h immersion in NaCl + AOT, the contact angle decreased due to further corrosion (70° ± 11); nevertheless, the contact angle remained higher than that of AZ31 immersed in the NaCl solution (13° ± 6). The contact angle measurements of samples are collected in Fig. 3(b). The same hydrophobic behavior was observed after immersion of AZ91D Mg alloy in oxalic acid solution containing AOT [34].

The principle underlying the hydrogen evolution test is based on the stoichiometry of Mg corrosion: the dissolution of one mole of Mg releases one mole of H_2 gas, as shown in Reaction (1) [51]. By monitoring the volume of evolved hydrogen, the corrosion rate of Mg can be effectively assessed.

The decreased evolved hydrogen and, consequently, the corrosion rate is vividly observed in Fig. 3(c). The amount of hydrogen evolution after 192 h of immersion in NaCl + AOT and NaCl is 0.37 ± 0.06 mL/cm^2 and 4.75 ± 0.37 mL/cm^2, respectively. The inhibition efficiency, calculated to be 92 % after 192 h using Equation (1), represents the effective corrosion inhibition performance of AOT for AZ31 Mg alloy.

4.1.3. Physical and chemical characteristics of surface

SEM images of the surfaces of immersion test samples were provided, displaying various immersion times of 1, 6, and 24 h. Additionally, the elemental compositional analysis of the starred point in Fig. 4(a), indicates the presence of sulfur (S) element after 1 h immersion in the NaCl + AOT solution which can be attributed to the adsorption of AOT on the surface.

Fig. 4(b) shows EDS from the surface of samples after immersion which represents the distribution of corrosion inhibitors and corrosion products. After 6 h, S and C elements related to the AOT can be found on the surface, representing the adsorption of inhibitor on AZ31 Mg alloy. Li et al. [52] previously reported the preferential adsorption of SDS in the Al-Mn intermetallic; however, our findings reveal a uniform distribution of the S element after both 6 and 24 h of immersion. Li et al.[52] also reported that the enhanced corrosion resistance of the samples after the addition of SDS to the NaCl solution is attributed to the incorporation of the inhibitor in the formed layer, as well as the modification of the microstructure and composition of the corrosion products which increases the compactness of the resulting oxide layer. It has also been claimed that the anionic nature of a surfactant can enhance the nucleation kinetics of positively charged $Mg(OH)_2$ nuclei, thus facilitating the formation of a denser corrosion product layer [53]. In a similar vein, the negatively charged AOT can induce a higher-density precipitation of $Mg(OH)_2$.

According to the XRD diagrams of the corroded surfaces after 5 days of immersion in both solutions (Fig. 5), the main corrosion product in both samples immersed in NaCl and NaCl + AOT is $Mg(OH)_2$ [54]. However, in the case of NaCl + AOT, the intensity of $Mg(OH)_2$ peaks are

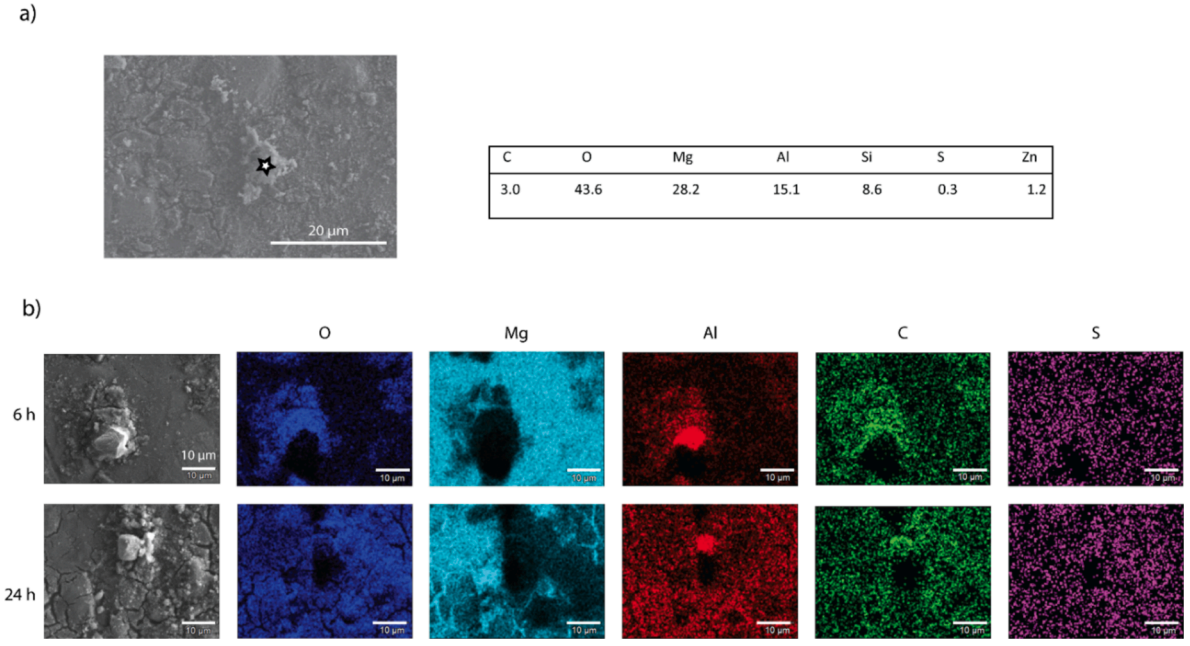

Fig. 4. a) SEM image and EDS (stared point) results of the substrate in NaCl + AOT solution after 1 h of immersion, b) EDS mapping of surface for substrate immersed in NaCl + AOT solution after 6 h and 24 h.

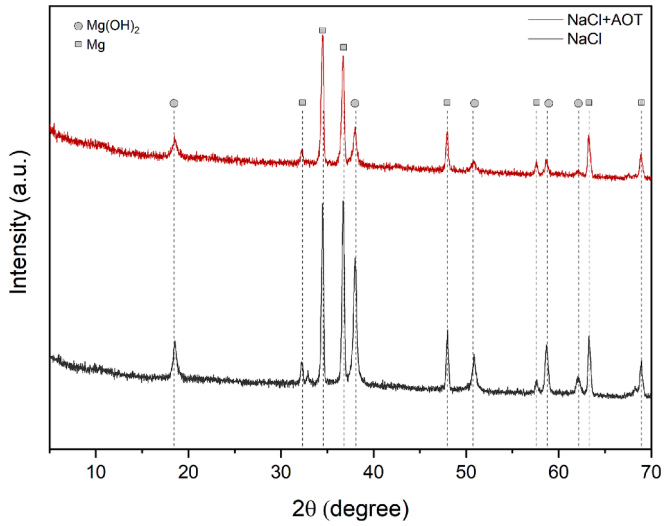

Fig. 5. XRD diagrams of samples in different solutions.

reduced, showing a decrease in the corrosion rate of Mg alloy [55].

To analyze the chemical state and elemental composition of the corrosion products, XPS measurements were conducted (Fig. 6). The survey spectrum obtained from the samples indicates the presence of O 1s, C 1s, Al 2p, Mg 2p, and Mg 2s in both NaCl and NaCl + AOT samples. The Mg 2p peak, with a binding energy of 49.5 eV, is assigned to Mg oxide and hydroxide in Mg^{2+} form [56,57]. Oxygen atoms (O 1s) in $Mg(OH)_2$ were found at 532 eV, suggesting that the corrosion products are mainly $Mg(OH)_2$ on the surface. The Al 2p peaks, with a binding energy of approximately 74 eV, can be attributed to Al oxide and hydroxide coming from the substrate [58]. According to Song et al. [59] corrosion products of AZ21 Mg alloy are mainly $Mg(OH)_2$ on the surface and Al_2O_3-rich compounds in the inner layer. C 1s peak at 285 eV can be related to the C–C or C–H groups due to inevitable contamination [57,58]. The binding energies related to the main peaks are reported in Table 1.

Fig. 6 demonstrates that the main distinction between the two samples immersed in NaCl and NaCl + AOT is the presence of the S 2p peak at 167.8 eV. This peak corresponds to the SO_3^- ion, the oxidized form of sulfur in AOT. It is the result of AOT adsorption after 1 h of immersion [52,60]. The peak for C 1s at a binding energy of 285 eV is associated with CH_2 hydrocarbons, while the higher binding energy peak (289 eV) is attributed to carbon bonded to AOT oxyfunctionalities, which can be another reason for the adsorption of this compound on the surface of Mg alloy [60]. These peaks are depicted in Fig. 7.

Table 1
The binding energies related to the main peaks of XPS.

Sample/ Binding energy (eV)	O 1s	C 1s	Al 2p	Mg 2s	S 2p
NaCl + AOT	532	285, 289	74.4	88.9	167.8
NaCl	532	285	74.6	89.2	–

4.1.4. DFT calculations

The DFT results show a strong interaction of the AOT with the metal surface, with a calculated interaction energy of −5.25 eV. This adsorption is realized by the interaction between the S group head of the AOT with the Mg surface, as suggested earlier in the text and shown in Fig. 8. Indeed, the S atom is localized on a hollow position with respect to the Mg surface with each of the three oxygen atoms pointing to a top Mg atom with an average Mg-O distance of 2.09 Å and a bond order of ~0.48 for each Mg-O bond. This is consistent with the experimental evidence showing the presence of the S atom on the surface. The large value of the interaction energy can also explain the experimental observation of a protective AOT film. The net charge of AOT adsorbed on the surface is q = −0.685 |e|, with the main part of this charge localized on the SO_3 head group with a value of q = −0.576 |e|. Note that the corresponding net charge computed on the free AOT(−)Na(+) salt is q = −0.782 |e| for the AOT part, which underlines a charge transfer during the adsorption process from the molecule to the metal; this favors a good adhesion by creating an attractive Coulomb interaction term. The localization of the negative charge on the anchoring unit can be considered as a good indicator of inhibitor efficiency since the anchor is involved in the interfacial charge transfer that stabilizes the adsorption and prevents the corrosion process [61,62].

4.2. Modification of LDH with AOT solution

4.2.1. Physical and chemical characteristics of LDH surface

LDH was immersed in a 0.1 M AOT solution (LDH + AOT) at a temperature of 60 °C for a duration of 18 h. According to the SEM images of the surface after immersing the LDH in an AOT solution (Fig. 9), it can be observed that the LDH structure has undergone changes, resulting in an increased lateral size of the LDH particles and a more uniform distribution throughout the surface. These alterations can be attributed to the structural rearrangement of the LDH induced by the presence of AOT and its long chain structure [35]. Moreover, the cross-section images of the LDH after immersion in the AOT solution (Fig. 9 (d)), reveals an increase in the thickness of the LDH inner layer from 11.8 ± 0.2 μm in LDH to 16.3 ± 0.3 μm in LDH + AOT. The increased thickness of this layer (which is mainly composed of $Mg(OH)_2$ [63]), along with its enhanced compactness, can be attributed to the adsorption of the AOT molecules, with their elongated chains, onto the substrate surface as well as increasing the wettability of the surface and

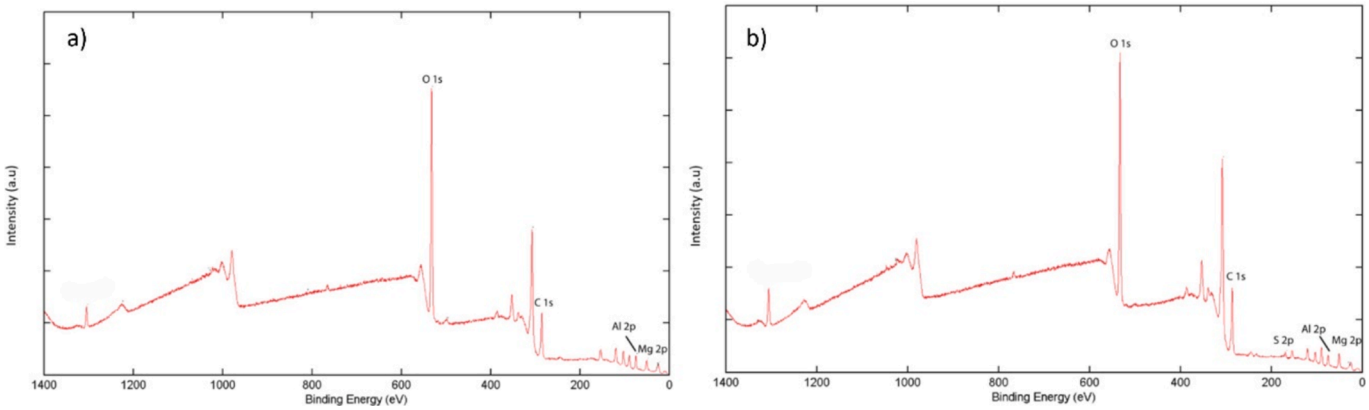

Fig. 6. XPS survey spectra of the samples after 1 h immersion in a) NaCl, and b) NaCl + AOT solutions.

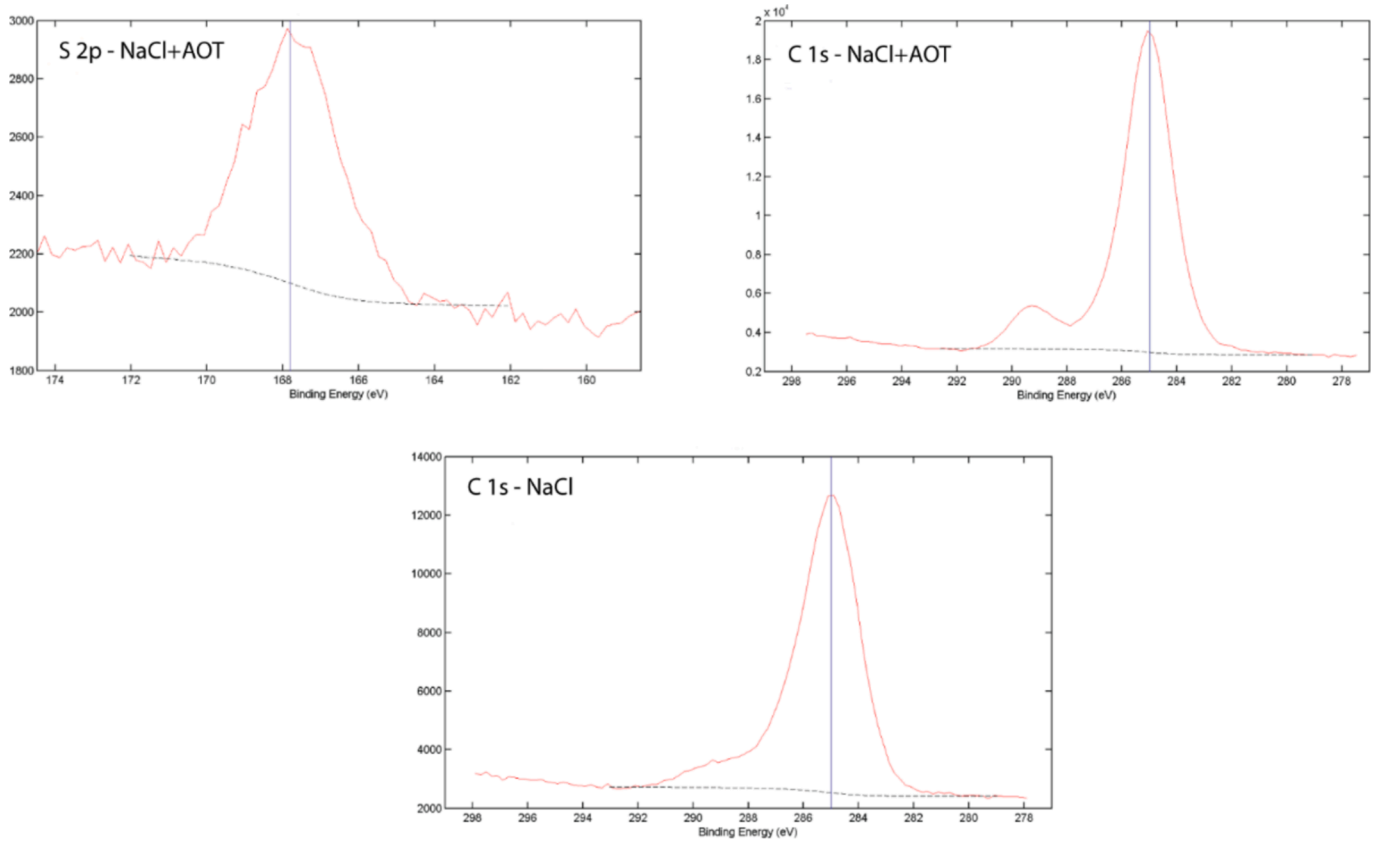

Fig. 7. XPS spectra (binding energy vs intensity (a.u)) related to S and C elements after 1 h immersion of the substrate in NaCl + AOT and NaCl solutions.

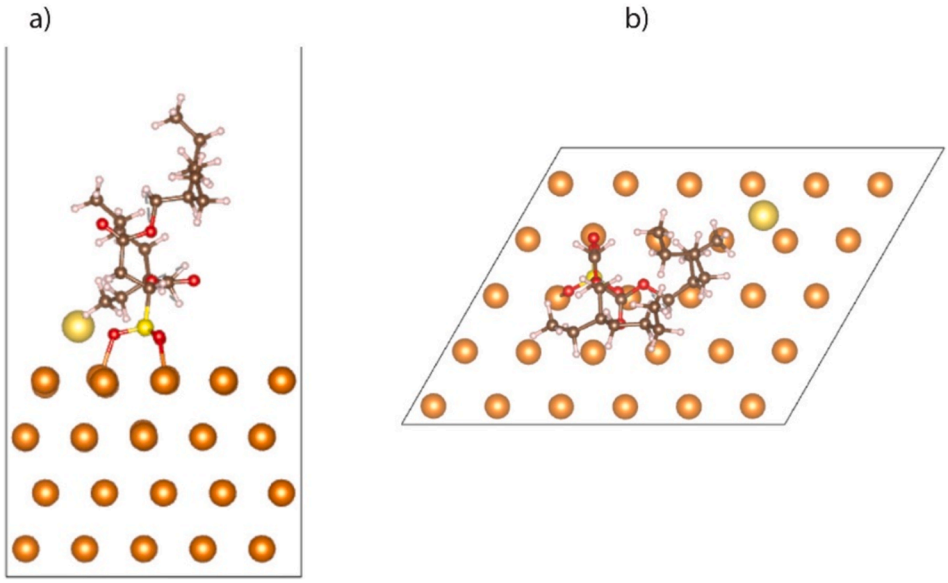

Fig. 8. a) Side, and b) top views of the computational models for the optimized adsorbed structure of AOT molecule onto the Mg substrate. the orange, red, brown, white, small, and big yellow balls stand for Mg, O, C, H, S, and Na atoms, respectively.

more dissolution of Mg substrate (release of Mg^{2+}). In our previous study [38], it was observed that a higher amount of Mg^{2+} leads to a thicker inner layer for LDH.

EDS mapping of the cross-section in Fig. 10 shows the concentrated Al element in the top layer representing the thickness of the LDH outer layer in both LDH samples that confirms maintenance of LDH structure even after immersion in AOT solution. Moreover, a small quantity of S element can be observed coming from AOT. The inner layer in both LDH samples is mainly composed of $Mg(OH)_2$ (higher thickness in the case of LDH + AOT). The existence of the anionic surfactants can change and modify the precipitation of $Mg(OH)_2$ and affect the nucleation and growth kinetics of $Mg(OH)_2$ which then results in the denser structure of LDH + AOT layer [64].

XRD was performed to study the crystalline structure of LDH and the

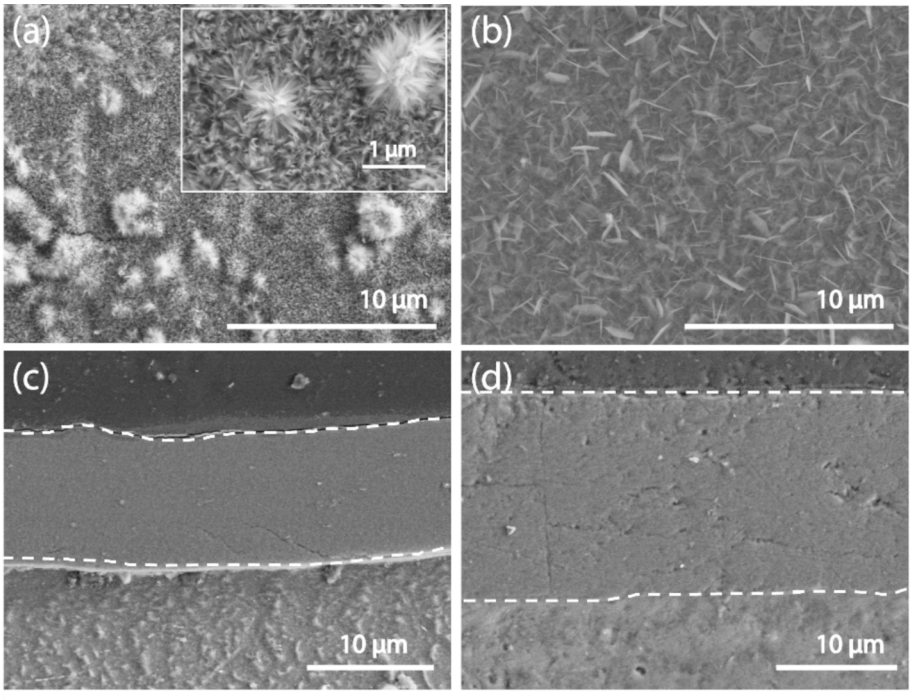

Fig. 9. SEM images of a) LDH, b) LDH + AOT surface, and c) LDH, d) LDH + AOT cross-section.

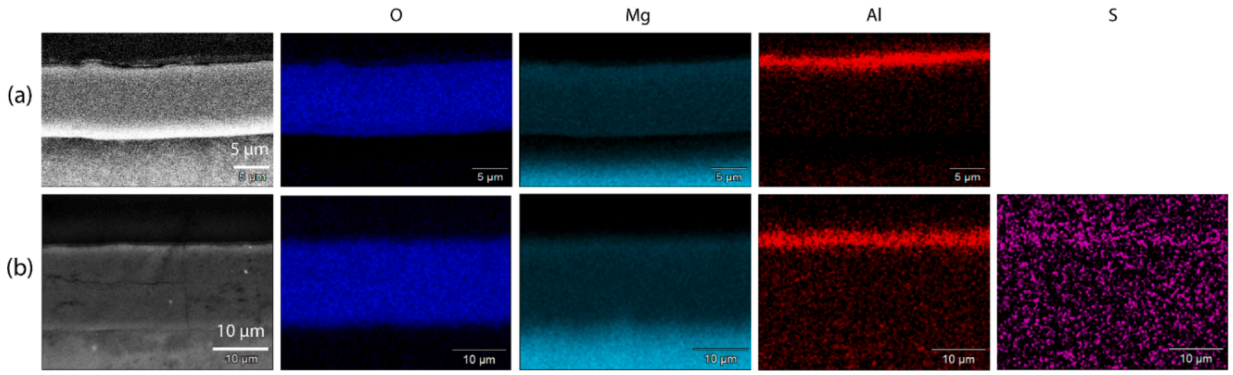

Fig. 10. EDS mapping from the cross-section of a) LDH, and b) LDH + AOT.

effect of AOT on it (Fig. 11). JCPDS No. 00-038-0478 was used to identify characteristic diffraction peaks of (003) and (006) LDH at 11.6° and 23.3°. Peaks at 18.43° and 38.02° related to $Mg(OH)_2$ are shown in the graphs in Fig. 11 using JCPDS No. 00-007-0239 that is attributed to the dissolution of Mg from the substrate for the formation of the LDH layer [38,65].

After immersion of LDH in AOT, the characteristic peaks of LDH (003) and (006) still exist and remain at the same position in the spectra of the LDH + AOT sample with increased intensity. Hence, we can infer that AOT had not been intercalated in the LDH layer; however, it modified the LDH structure to a denser and more compact layer.

Water contact angle measurements were also performed after modification of LDH with AOT. It was observed that AOT affects the surface of LDH by making it less hydrophilic with contact angles of 50° + 6 and 15° + 5, after and before treatment with AOT, respectively. In general, LDH conversion coatings increase the hydrophilicity of the surface in comparison to bare substrates [66]. AOT has the ability to reduce the hydrophilicity of LDH surfaces by altering their structure and morphology [67]. Furthermore, the inclusion of a hydrophobic alkyl chain of this compound can be effective in decreasing the hydrophilicity of LDH [34]. Hydrophobic surfaces are effective in preventing corrosion for longer periods of time [68].

4.2.2. *Electrochemical investigations*

EIS measurements were conducted to examine the impact of AOT on the corrosion resistance of the LDH coating. As shown in Fig. 12, the overall impedance modulus of LDH + AOT at a low frequency (0.1 Hz) is seven times higher than that of pure LDH after one hour of immersion, indicating the anti-corrosion effect of AOT on LDH. In this figure, the EIS results of bare Mg alloy are shown as a reference for investigating the influence of LDH layers. Both LDH samples exhibit a phase angle of around −50° at high frequency, indicating the protective nature of the films. This suggests that the addition of AOT does not alter the protective properties of the outer LDH layer, but it enhances the corrosion resistance of the LDH inner layer, as evidenced by the overall increase in impedance.

As depicted in Fig. 12, LDH + AOT exhibits higher impedance compared to LDH across different immersion times. Notably, after 24 h immersion in the saline solution, a noticeable increase in the impedance value is observed that can be attributed to the corrosion inhibition of AOT. After 24 h immersion, the middle-frequency time constant appears at a frequency range between 10^0 and 10^3 Hz for both LDH samples.

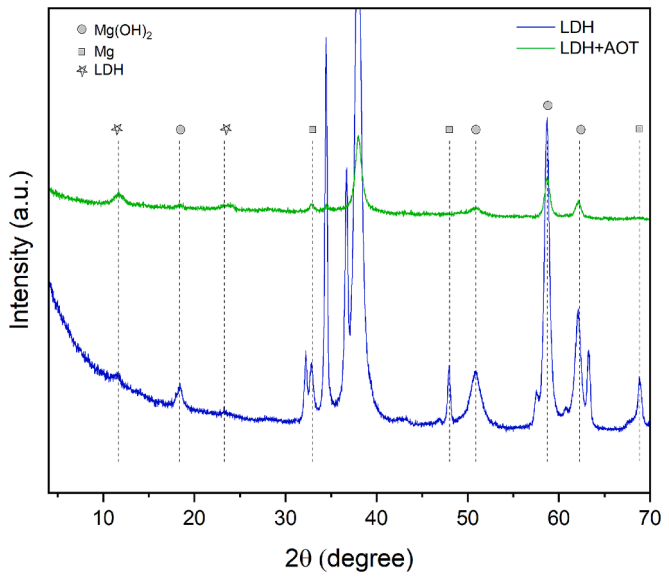

Fig. 11. XRD diagrams of LDH samples.

However, in the case of LDH + AOT, an additional time constant is observed at low frequency (<10^0 Hz), which can be ascribed to the increased corrosion resistance provided by AOT and its corrosion-inhibiting effect. The production of a thin protective layer between the inorganic coating (LDH here) and the substrate was also observed in previous studies with PEO and decylphosphonate sodium salt and with a thickness of less than 1 μm [22]. For this reason, the equivalent circuit in Fig. 13(a) was used for fitting EIS data. In this circuit, the subscripts "out" and "in" are used to represent the outer and inner LDH layers, respectively [38,39]. R_f and CPE_f are related to the resistance and capacitance behavior caused by the AOT effect.

The electrical circuit depicted in Fig. 13(b) was employed to fit EIS data of LDH after 1 h and 24 h; however, after 168 h, the inductive loop was added due to the non-stationary of the system with passing time (Fig. 13(c)) [69]. In these circuits, CPE_{dl}, and R_{ct} represent the response of the substrate-electrolyte interface capacitance and the charge transfer resistance, respectively [70,71]. Table 2 lists the fitting data of samples at different immersion times. The mechanism of corrosion mainly involves charge transfer; therefore, R_{ct} can be used for comparing the corrosion resistance of samples [35]. The fitting results show that the value of R_{ct} decreases as the immersion time increases, indicating a decline in the corrosion resistance of the coatings (Table 2).

As mentioned in the previous section, the morphology of LDH was altered through the modification by AOT. This resulted in a LDH with a thicker inner layer (Fig. 9). According to Equation (3), where ε, $ε_0$, A, and d represent the dielectric constant of the medium and space, testing area, and distance, respectively [72], a higher thickness of the inner layer (d in Equation (3)) leads to a decrease in the corresponding capacitance value (C). This finding aligns with the fitting results in which a lower capacitance value for the inner layer is observed for LDH + AOT sample (Table 2).

$$C = \varepsilon\varepsilon_0 A/d \quad (3$$

4.2.3. H_2 evolution test

An additional technique was employed to further investigate the long-term corrosion behaviour of LDH modified with AOT during immersion in 0.1 M NaCl solution. Fig. 14 presents the volume of hydrogen gas evolved after 198 h of immersion for LDH and LDH + AOT samples. The results indicate a reduction in hydrogen evolution for the LDH-coated samples compared to the bare Mg alloy during the whole immersion time. Notably, the LDH + AOT sample exhibits the lowest hydrogen evolution over the entire immersion time (198 h) with a value of 0.65 ± 0.02 mL/cm^2. This value is lower than the amount of evolved hydrogen observed for LDH (with a value of 1 ± 0.02 mL/cm^2, about 1.5

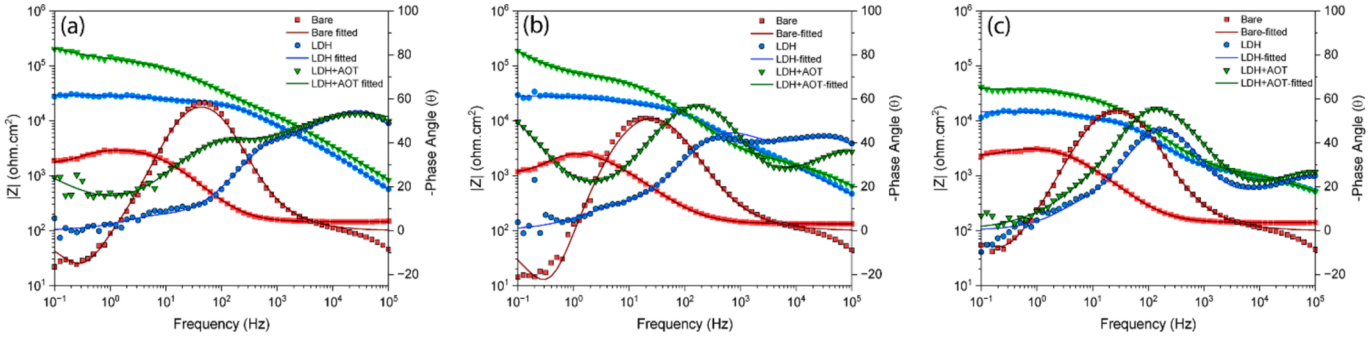

Fig. 12. Bode plots of EIS spectra for samples after a) 1 h, b) 24 h, c) 168 h immersion.

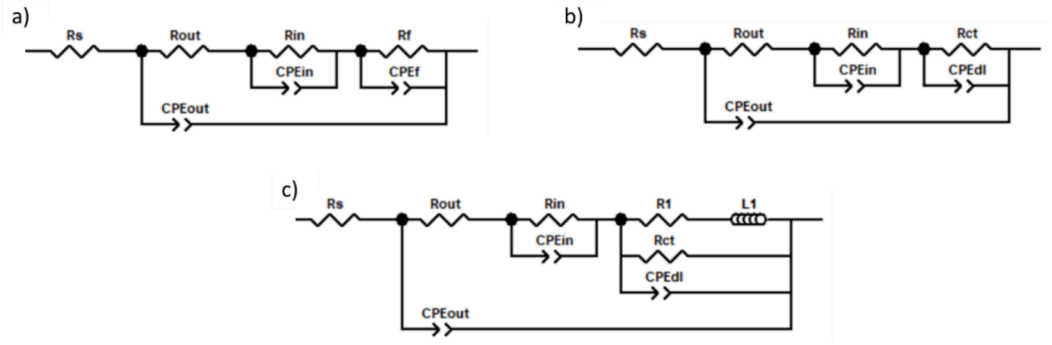

Fig. 13. Equivalent circuits for the fitting of EIS data.

Table 2
Fitting results obtained from EIS diagrams for samples at different immersion times.

Sample	R_{out} ($\Omega \cdot cm^2$)	CPE_{out} ($\Omega^{-1} \cdot s^n \cdot cm^{-2}$)	n	R_{in} ($\Omega \cdot cm^2$)	CPE_{in} ($\Omega^{-1} \cdot s^n \cdot cm^{-2}$)	n	R_{ct}/R_f ($\Omega \cdot cm^2$)	CPE_{dl}/CPE_f ($\Omega^{-1} \cdot s^n \cdot cm^{-2}$)	n
LDH-1 h	5730	5.8×10^{-8}	0.78	19518	3.1×10^{-7}	0.65	3683	8.5×10^{-6}	0.99
LDH-24 h	4864	6.08×10^{-7}	0.63	18225	9.6×10^{-8}	0.85	5030	8.4×10^{-6}	0.99
LDH-168 h	1187	7.61×10^{-7}	0.65	11483	6.6×10^{-7}	0.84	2384	7.6×10^{-5}	0.95
LDH + AOT-1 h	22404	4.6×10^{-8}	0.7	101870	2.8×10^{-7}	0.68	1.5×10^{6}	1.1×10^{-5}	0.6
LDH + AOT-24 h	3006	5.1×10^{-8}	0.6	58254	7.5×10^{-8}	0.91	9.1×10^{5}	7.7×10^{-6}	0.72
LDH + AOT-168 h	963	1.6×10^{-7}	0.73	28,155	5.7×10^{-7}	0.81	9207	1.2×10^{-5}	0.8

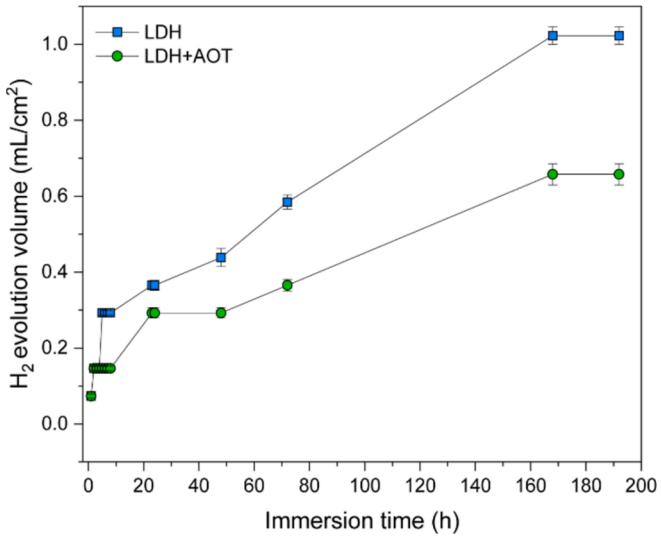

Fig. 14. Hydrogen evolution volume for LDH and LDH + AOT samples during different immersion times.

times higher) and the bare substrate (4.75 ± 0.37 mL/cm^2, approximately 7 times higher). These results demonstrate the effectiveness of AOT incorporation in providing prolonged corrosion inhibition, which is in agreement with EIS results.

To summarize, it can be stated that the immersion of LDH in an AOT solution alters the structure and morphology of the LDH outer layer, increases LDH inner layer thickness and compactness, increases the water contact angle, and, therefore, improves the corrosion resistance of the whole substrate system.

It was shown in our previous study [39] that LDH is effective in the adhesion of organic coatings to substrates, thereby leading to improved corrosion resistance. AOT as a surfactant comprising both organic and inorganic parts can act as a bridge between the organic coating and the substrate (or inorganic coatings such as PEO or LDH). Consequently, the incorporation of AOT with LDH may offer significant advantages, especially in the application of organic coatings (such as benzoxazine [73]), which will be the subject of a separate study.

5. Conclusion

The present study provides a detailed investigation into the corrosion inhibition properties of AOT on AZ31 Mg alloy through a combination of EIS and immersion tests as well as advanced surface characterization techniques. It was observed that the corrosion rate decreased using AOT by forming a film that could prevent corrosion. Moreover, DFT calculations showed a high interaction energy for the adsorption of AOT on the Mg alloy substrate. After confirming the corrosion inhibition effect of AOT for Mg alloy, a saturated solution of this surfactant was prepared to be further used for LDH immersion and its incorporation into LDH structure. Physical and chemical characterizations of modified LDH with AOT confirmed the existence of LDH after immersion in AOT solution. It was also observed that AOT could enhance the corrosion resistance of Mg alloy by forming a thicker LDH (inner) layer, which was confirmed by SEM images. The modification of LDH with AOT could enhance the corrosion resistance of the substrate, which can be used as a surface pretreatment for further application of organic coatings.

CRediT authorship contribution statement

Roya Malekkhouyan: Writing – original draft, Methodology, Investigation, Formal analysis, Conceptualization. **Yoann Paint:** Validation, Investigation. **Xavier Noirfalise:** Validation, Investigation. **Maurice Gonon:** Validation, Investigation. **David Cornil:** Software, Methodology, Investigation, Conceptualization. **Jérôme Cornil:** Validation, Supervision. **Marie-Georges Olivier:** Writing – review & editing, Validation, Supervision, Funding acquisition, Conceptualization.

Declaration of competing interest

The authors declare that they have no known competing financial interests or personal relationships that could have appeared to influence the work reported in this paper.

Acknowledgements

The authors would like to thank UMONS (University of Mons) for the financial support in the framework of the ARC 2020 (Action de Recherche Collective) PROCOMAG project attributed by the Fédération Wallonie-Bruxelles and the Fund for Scientific Research (F.R.S) of FNRS within the Consortium des Equipements de Calcul Intensif (CECI) under grant 2.5020.11 by the Walloon Region (Lucia Tier-1 supercomputer) under grant 1117545. J.C. which is an FNRS research director.

Data availability

Data will be made available on request.

References

[1] T. Wu, K. Zhang, Corrosion and protection of magnesium alloys: Recent advances and future perspectives, Coatings 13 (9) (2023) 1533, https://doi.org/10.3390/coatings13091533.
[2] M. Esmaily, J.E. Svensson, S. Fajardo, N. Birbilis, G.S. Frankel, S. Virtanen, R. Arrabal, S. Thomas, L.G. Johansson, Fundamentals and advances in magnesium alloy corrosion, Prog. Mater Sci. 89 (2017) 92–193, https://doi.org/10.1016/j.pmatsci.2017.04.011.
[3] J. Song, J. She, D. Chen, F. Pan, Latest research advances on magnesium and magnesium alloys worldwide, J. Magnesium Alloys 8 (1) (2020) 1–41, https://doi.org/10.1016/j.jma.2020.02.003.
[4] P. Gore, T.W. Cain, J. Laird, J. Scully, N. Birbilis, V. Raja, Enrichment efficiency of noble alloying elements on magnesium and effect on hydrogen evolution, Corros. Sci. 151 (2019) 206–218, https://doi.org/10.1016/j.corsci.2019.02.026.
[5] W. Wu, Z. Wang, S. Zang, X. Yu, H. Yang, S. Chang, Research progress on surface treatments of biodegradable mg alloys: A review, ACS Omega 5 (2) (2020) 941–947, https://doi.org/10.1021/acsomega.9b03423.
[6] Y. Kang, S. Yan, Z. Li, Z. Wang, A. Yang, W. Ma, W. Chen, Y. Qu, Influence of Anodic oxidation on the organizational structure and corrosion resistance of oxide film on AZ31B magnesium alloy, Coatings 14 (3) (2024) 271, https://doi.org/10.3390/coatings14030271.

[7] M. Han, J. Du, Y. Chen, Q. Sun, K. Hu, Influence of ultrasonic shot peening on the microstructure and corrosion behavior of AZ80M magnesium alloy, J. Alloy. Compd. 980 (2024) 173633, https://doi.org/10.1016/j.jallcom.2024.173633.
[8] M. Wu, L. Wu, R. Wang, A. Wang, X. Dai, W. Yao, Y. Yuan, A. Andrej, J. Wang, F. Pan, Preparation and corrosion behavior of layered double hydroxides-graphene oxide composite coatings modified by sodium dodecylbenzene sulfonate on the surface of AZ31 Mg alloy, Smart Mater. Manuf. (2024) 100054, https://doi.org/10.1016/j.smmf.2024.100054.
[9] S. Cheng, L. Lan, M. Li, X. Chu, H. Zhong, M. Yao, F. Peng, Y. Zhang, Pure Mg–Al layered double hydroxide film on magnesium alloys for orthopedic applications, ACS Omega 6 (38) (2021) 24575–24584, https://doi.org/10.1021/acsomega.1c03169.
[10] L. Wu, D. Yang, G. Zhang, Z. Zhang, S. Zhang, A. Tang, F. Pan, Fabrication and characterization of Mg-M layered double hydroxide films on anodized magnesium alloy AZ31, Appl. Surf. Sci. 431 (2018) 177–186, https://doi.org/10.1016/j.apsusc.2017.06.244.
[11] F. de Sousa Santos, L. Binder, N. Scharnagl, T.F. da Conceição, Sustainable smart coatings of chitosan and LDH loaded with natural inhibitors for corrosion protection of Mg AZ31 alloy, Colloids Surf A Physic. Eng Asp 688 (2024) 133639, https://doi.org/10.1016/j.colsurfa.2024.133639.
[12] G. Shen, J. Kong, Y. Fei, L. Xu, L. Zhang, X. Jie, D. Ning, Z. Chen, Zn/Ni composite coating modified by reduced graphene oxide and layered double hydroxide with synergistic effect for superior corrosion protection of Mg alloys, Appl. Surf. Sci. 645 (2024) 158849, https://doi.org/10.1016/j.apsusc.2023.158849.
[13] Z. Chen, Q. Fan, M. Huang, H. Cölfen, Synthesis of two-dimensional layered double hydroxides: A systematic overview, CrstEngComm 24 (26) (2022) 4639–4655, https://doi.org/10.1039/d2ce00511e.
[14] D. Chaillot, S. Bennici, J. Brendle, Layered double hydroxides and LDH-derived materials in chosen environmental applications: A review, Environ. Sci. Pollut Res. Int. 28 (19) (2021) 24375–24405, https://doi.org/10.1007/s11356-020-08498-6.
[15] Y. Kuang, L. Zhao, S. Zhang, F. Zhang, M. Dong, S. Xu, Morphologies, preparations and applications of layered double hydroxide micro-/nanostructures, Materials 3 (12) (2010) 5220–5235, https://doi.org/10.3390/ma3125220.
[16] N.G.B. Allou, P. Saikia, A. Borah, R.L. Goswamee, Hybrid nanocomposites of layered double hydroxides: an update of their biological applications and future prospects, Colloid Polym. Sci. 295 (5) (2017) 725–747, https://doi.org/10.1007/s00396-017-4047-3.
[17] J. Zhang, D. Lian, J. Li, M. Zhang, Z. Wang, J. Wu, C. Wang, Effect of different anion intercalations on the corrosion resistance of layered double hydroxides on the surface of LA43M, Mater. Corros. 75 (3) (2024) 398–408, https://doi.org/10.1002/maco.202314017.
[18] P.R. Roberge, Handbook of corrosion engineering, McGraw-Hill Education, 2019.
[19] X. Zhou, Q. Dong, D. Wei, J. Bai, F. Xue, B. Zhang, Z. Ba, Z. Wang, Smart corrosion inhibitors for controlled release: A review, Corros. Eng. Sci. Technol. 58 (2) (2022) 190–204, https://doi.org/10.1080/1478422x.2022.2161122.
[20] R. Ganjoo, A. Kumar, Current Trends in anti-corrosion studies of surfactants on metals and alloys, J. Bio- Tribo-Corrosion 8 (1) (2021), https://doi.org/10.1007/s40735-021-00597-2.
[21] S.A. Umoren, M.T. Abdullahi, M.M. Solomon, An overview on the use of corrosion inhibitors for the corrosion control of Mg and its alloys in diverse media, J. Mater. Res. Technol. 20 (2022) 2060–2093, https://doi.org/10.1016/j.jmrt.2022.08.021.
[22] B. Vaghefinazari, E. Wierzbicka, P. Visser, R. Posner, R. Arrabal, E. Matykina, M. Mohedano, C. Blawert, M.L. Zheludkevich, S.V. Lamaka, Chromate-free corrosion protection strategies for magnesium alloys-A review: Part III-corrosion inhibitors and combining them with other protection strategies, Materials (Basel) 15 (23) (2022), https://doi.org/10.3390/ma15238489.
[23] X. Lu, Y. Li, P. Ju, Y. Chen, J. Yang, K. Qian, T. Zhang, F. Wang, Unveiling the inhibition mechanism of an effective inhibitor for AZ91 Mg alloy, Corros. Sci. 148 (2019) 264–271, https://doi.org/10.1016/j.corsci.2018.12.025.
[24] S.V. Lamaka, B. Vaghefinazari, D. Mei, R.P. Petrauskas, D. Höche, M. L. Zheludkevich, Comprehensive screening of Mg corrosion inhibitors, Corros. Sci. 128 (2017) 224–240, https://doi.org/10.1016/j.corsci.2017.07.011.
[25] E. Rocca, J. Steinmetz, Inhibition of lead corrosion with saturated linear aliphatic chain monocarboxylates of sodium, Corros. Sci. 43 (5) (2001) 891–902, https://doi.org/10.1016/S0010-938X(00)00115-3.
[26] S.F.A. El-Aziz, A.M. Al-Bonayan, M. Eissa, D.M. Eid, Electrochemical and quantum chemical studies on the corrosion inhibition of 1037 carbon steel by different types of surfactants, RSC Adv. 12 (6) (2022) 3253–3273, https://doi.org/10.1039/d1ra07983b.
[27] H. Song, Z. Xu, L. Benabou, Z. Yin, H. Guan, H. Yan, L. Chao, Z. Hu, X. Wang, Sodium dodecyl sulfate (SDS) as an effective corrosion inhibitor for Mg-8Li-3Al alloy in aqueous NaCl: A combined experimental and theoretical investigation, J. Magnesium Alloys 11 (1) (2023) 287–300, https://doi.org/10.1016/j.jma.2021.07.006.
[28] A. Frignani, V. Grassi, F. Zanotto, F. Zucchi, Inhibition of AZ31 Mg alloy corrosion by anionic surfactants, Corros. Sci. 63 (2012) 29–39, https://doi.org/10.1016/j.corsci.2012.05.012.
[29] Y. Song, H. Wang, Q. Liu, G. Li, S. Wang, X. Zhu, Sodium dodecyl sulfate (SDS) intercalated Mg Al layered double hydroxides film to enhance the corrosion resistance of AZ31 magnesium alloy, Surf. Coat. Technol. 422 (2021), https://doi.org/10.1016/j.surfcoat.2021.127524.
[30] J. Chen, J. He, L. Li, Spectroscopic insight into the role of SDBS on the interface evolution of Mg in NaCl corrosive medium, Corros. Sci. 182 (2021), https://doi.org/10.1016/j.corsci.2020.109215.
[31] M. Askari, M. Aliofkhazraei, R. Jafari, P. Hamghalam, A. Hajizadeh, Downhole corrosion inhibitors for oil and gas production – A review, Appl. Surf. Sci. Adv. 6 (2021), https://doi.org/10.1016/j.apsadv.2021.100128.
[32] T. Kevin, K.L.N. Fitzgerald, Small Animal Toxicology (Third Edition). 2013. Chapter 20 - Poisonings in the Captive Reptile: p. 229-249. https://doi.org/10.1016/B978-1-4557-0717-1.00020-X.
[33] R. Ganjoo, S. Sharma, A. Thakur, A. Kumar, Thermodynamic study of corrosion inhibition of Dioctylsulfosuccinate Sodium Salt as corrosion inhibitor against mild steel in 1 M HCl, Mater. Today Proc. 66 (2022) 529–533, https://doi.org/10.1016/j.matpr.2022.05.594.
[34] S. Liu, L. Luo, H. Huang, G. Huang, Efficient and long-lasting corrosion inhibition mechanism of an anionic surfactant on AZ91D Mg alloy in oxalic acid solution, J. Mater. Res. Technol. 28 (2024) 2876–2886, https://doi.org/10.1016/j.jmrt.2023.12.221.
[35] M. Huang, G. Lu, J. Pu, Y. Qiang, Superhydrophobic and smart MgAl-LDH anti-corrosion coating on AZ31 Mg surface, J. Ind. Eng. Chem. 103 (2021) 154–164, https://doi.org/10.1016/j.jiec.2021.07.031.
[36] J. Chen, L. Fang, F. Wu, J. Xie, J. Hu, B. Jiang, H. Luo, Corrosion resistance of a self-healing rose-like MgAl-LDH coating intercalated with aspartic acid on AZ31 Mg alloy, Prog. Org. Coat. 136 (2019) 105234, https://doi.org/10.1016/j.porgcoat.2019.105234.
[37] Y. Song, Y. Tang, L. Fang, F. Wu, X. Zeng, J. Hu, S.F. Zhang, B. Jiang, H. Luo, Enhancement of corrosion resistance of AZ31 Mg alloys by one-step in situ synthesis of ZnAl-LDH films intercalated with organic anions (ASP, La), J. Magnesium Alloys 9 (2) (2021) 658–667, https://doi.org/10.1016/j.jma.2020.03.013.
[38] R. Malekkhouyan, Y. Paint, L. Prince, M. Gonon, M.-G. Olivier, Controlling lateral size and thickness of layered double hydroxide (LDH) used as conversion layer for corrosion protection of AZ31 Mg alloy, Corro. Mater. Degradation 4 (1) (2023) 174–195, https://doi.org/10.3390/cmd4010011.
[39] R. Malekkhouyan, L. Van Renterghem, L. Bonnaud, Y. Paint, M. Gonon, D. Cornil, J. Cornil, J.-M. Raquez, M.-G. Olivier, Effect of surface pretreatment on the production of LDH for post-treatment with benzoxazine resin, Surf. Coat. Technol. 479 (2024), https://doi.org/10.1016/j.surfcoat.2024.130538.
[40] I.M. Umlong, K. Ismail, Micellization of AOT in aqueous sodium chloride, sodium acetate, sodium propionate, and sodium butyrate media: a case of two different concentration regions of counterion binding, J. Colloid Interface Sci. 291 (2) (2005) 529–536, https://doi.org/10.1016/j.jcis.2005.05.003.
[41] G. Kresse, D. Joubert, From ultrasoft pseudopotentials to the projector augmented-wave method, Phys. Rev. B 59 (3) (1999) 1758–1775, https://doi.org/10.1103/PhysRevB.59.1758.
[42] G. Kresse, J. Furthmüller, Efficient iterative schemes for ab initio total-energy calculations using a plane-wave basis set, Phys. Rev. B 54 (16) (1996) 11169–11186, https://doi.org/10.1103/PhysRevB.54.11169.
[43] J.P. Perdew, K. Burke, M. Ernzerhof, Generalized gradient approximation made simple, Phys. Rev. Lett. 77 (18) (1996) 3865–3868, https://doi.org/10.1103/PhysRevLett.77.3865.
[44] S. Grimme, J. Antony, S. Ehrlich, H. Krieg, A consistent and accurate ab initio parametrization of density functional dispersion correction (DFT-D) for the 94 elements H-Pu, J. Chem. Phys. 132 (15) (2010), https://doi.org/10.1063/1.3382344.
[45] S. Grimme, S. Ehrlich, L. Goerigk, Effect of the damping function in dispersion corrected density functional theory, J. Comput. Chem. 32 (7) (2011) 1456–1465, https://doi.org/10.1002/jcc.21759.
[46] T.A. Manz, N.G. Limas, IntroducingDDEC6 atomic population analysis: part 1. Charge partitioning theory and methodology, RSC Adv. 6 (53) (2016) 47771–47801, https://doi.org/10.1039/C6RA04656H.
[47] L. Wang, D. Snihirova, M. Deng, C. Wang, B. Vaghefinazari, G. Wiese, M. Langridge, D. Höche, S.V. Lamaka, M.L. Zheludkevich, Insight into physical interpretation of high frequency time constant in electrochemical impedance spectra of Mg, Corros. Sci. 187 (2021), https://doi.org/10.1016/j.corsci.2021.109501.
[48] L. Wang, D. Snihirova, M.D. Havigh, M. Deng, S.V. Lamaka, H. Terryn, M. L. Zheludkevich, Non-stationarity in electrochemical impedance measurement of Mg-based materials in aqueous media, Electrochim. Acta 468 (2023), https://doi.org/10.1016/j.electacta.2023.143140.
[49] G.-L. Song, A. Atrens, Recently deepened insights regarding Mg corrosion and advanced engineering applications of Mg alloys, J. Magnesium Alloys 11 (11) (2023) 3948–3991, https://doi.org/10.1016/j.jma.2023.08.012.
[50] G.-L. Song, M. Liu, The effect of Mg alloy substrate on “electroless” E-coating performance, Corros. Sci. 53 (11) (2011) 3500–3508, https://doi.org/10.1016/j.corsci.2011.06.016.
[51] G. Song, A. Atrens, D. StJohn, An hydrogen evolution method for the estimation of the corrosion rate of magnesium alloys, in Essential readings in magnesium technology. Springer (2016) 565–572, https://doi.org/10.1002/9781118805497.ch44.
[52] Y. Li, X. Lu, K. Wu, L. Yang, T. Zhang, F. Wang, Exploration the inhibition mechanism of sodium dodecyl sulfate on Mg alloy, Corros. Sci. 168 (2020), https://doi.org/10.1016/j.corsci.2020.108559.
[53] Y. Cui, T. Zhang, F. Wang, New understanding on the mechanism of organic inhibitors for magnesium alloy, Corros. Sci. 198 (2022), https://doi.org/10.1016/j.corsci.2022.110118.
[54] S. Feliu Jr, I. Llorente, Corrosion product layers on magnesium alloys AZ31 and AZ61: Surface chemistry and protective ability, Appl. Surf. Sci. 347 (2015) 736–746, https://doi.org/10.1016/j.apsusc.2015.04.189.

[55] B. Vaghefinazari, S.V. Lamaka, E. Gazenbiller, K. Yasakau, C. Blawert, M. Serdechnova, N. Scharnagl, D.C.F. Wieland, M.L. Zheludkevich, Corrosion inhibition of decylphosphonate on bare and PEO-coated Mg alloy, Corros. Sci. 226 (2024), https://doi.org/10.1016/j.corsci.2023.111651.
[56] H. Yao, Y. Li, A. Wee, An XPS investigation of the oxidation/corrosion of melt-spun Mg, Appl. Surf. Sci. 158 (1–2) (2000) 112–119, https://doi.org/10.1016/S0169-4332(99)00593-0.
[57] L. Wang, T. Shinohara, B.-P. Zhang, XPS study of the surface chemistry on AZ31 and AZ91 magnesium alloys in dilute NaCl solution, Appl. Surf. Sci. 256 (20) (2010) 5807–5812, https://doi.org/10.1016/j.apsusc.2010.02.058.
[58] M. Liu, S. Zanna, H. Ardelean, I. Frateur, P. Schmutz, G. Song, A. Atrens, P. Marcus, A first quantitative XPS study of the surface films formed, by exposure to water, on Mg and on the Mg–Al intermetallics: Al3Mg2 and Mg17Al12, Corros. Sci. 51 (5) (2009) 1115–1127, https://doi.org/10.1016/j.corsci.2009.02.017.
[59] G. Song, A. Atrens, X. Wu, B. Zhang, Corrosion behaviour of AZ21, AZ501 and AZ91 in sodium chloride, Corros. Sci. 40 (10) (1998) 1769–1791, https://doi.org/10.1016/S0010-938X(98)00078-X.
[60] G. Hota, S.B. Idage, K.C. Khilar, Characterization of nano-sized CdS–Ag2S core-shell nanoparticles using XPS technique, Colloids Surf. A Physicochem. Eng. Asp 293 (1–3) (2007) 5–12, https://doi.org/10.1016/j.colsurfa.2006.06.036.
[61] M. Esmaeilzadeh Khabazi, A. Najafi Chermahini, DFT study on corrosion inhibition by tetrazole derivatives: Investigation of the substitution effect, ACS Omega 8 (11) (2023) 9978–9994, https://doi.org/10.1021/acsomega.2c07185.
[62] Z. Cao, Y. Tang, H. Cang, J. Xu, G. Lu, W. Jing, Novel benzimidazole derivatives as corrosion inhibitors of mild steel in the acidic media. Part II: theoretical studies, Corrosion Sci. 83 (2014) 292–298, https://doi.org/10.1016/j.corsci.2014.02.025.
[63] F. Shi, J. Zhao, M. Tabish, J. Wang, P. Liu, J. Chang, One-step hydrothermal synthesis of 2, 5-PDCA-containing MgAl-LDHs three-layer composite coating with high corrosion resistance on AZ31, J. Magnesium Alloys 11 (7) (2023) 2541–2557, https://doi.org/10.1016/j.jma.2022.05.017.
[64] Y. Gao, H. Wang, Y. Su, Q. Shen, D. Wang, Influence of magnesium source on the crystallization behaviors of magnesium hydroxide, J. Cryst. Growth 310 (16) (2008) 3771–3778, https://doi.org/10.1016/j.jcrysgro.2008.05.032.
[65] L. Wu, F. Pan, Y. Liu, G. Zhang, A. Tang, A. Atrens, Influence of pH on the growth behaviour of Mg–Al LDH films, Surf. Eng. 34 (9) (2018) 674–681, https://doi.org/10.1080/02670844.2017.1382062.
[66] V. Kasneryk, M. Serdechnova, C. Blawert, M.L. Zheludkevich, LDH has been grown: What is next? Overview on methods of post-treatment of LDH conversion coatings, Appl. Clay Sci. 232 (2023), https://doi.org/10.1016/j.clay.2022.106774.
[67] F. Zhang, L. Zhao, H. Chen, S. Xu, D.G. Evans, X. Duan, Corrosion resistance of superhydrophobic layered double hydroxide films on aluminum, Angew. Chem. 120 (13) (2008) 2500–2503, https://doi.org/10.1002/ange.200704694.
[68] Y. Li, S. Li, Y. Zhang, M. Yu, J. Liu, Fabrication of superhydrophobic layered double hydroxides films with different metal cations on anodized aluminum 2198 alloy, Mater. Lett. 142 (2015) 137–140, https://doi.org/10.1016/j.matlet.2014.11.148.
[69] L. Wang, D. Snihirova, M.D. Havigh, M. Deng, S.V. Lamaka, H. Terryn, M. L. Zheludkevich, Non-stationarity in electrochemical impedance measurement of Mg-based materials in aqueous media, Electrochim. Acta 468 (2023) 143140, https://doi.org/10.1016/j.electacta.2023.143140.
[70] S.V. Gnedenkov, S.L. Sinebryukhov, V.I. Sergienko, Electrochemical impedance simulation of a metal oxide heterostructure/electrolyte interface: A review, Russ. J. Electrochem. 42 (3) (2006) 197–211, https://doi.org/10.1134/s1023193506030013.
[71] X. Dai, L. Wu, Y. Xia, Y. Chen, Y. Zhang, B. Jiang, Z. Xie, W. Ci, G. Zhang, F. Pan, Intercalation of Y in Mg-Al layered double hydroxide films on anodized AZ31 and Mg-Y alloys to influence corrosion protective performance, Appl. Surf. Sci. 551 (2021) 149432, https://doi.org/10.1016/j.apsusc.2021.149432.
[72] F. Deflorian, L. Fedrizzi, S. Rossi, P. Bonora, Organic coating capacitance measurement by EIS: Ideal and actual trends, Electrochim. Acta 44 (24) (1999) 4243–4249, https://doi.org/10.1016/S0013-4686(99)00139-5.
[73] L. Van Renterghem, R. Malekkhouyan, L. Bonnaud, R. Tavernier, M. Olivier, J.-M. Raquez, Solvent-free coatings based on bio-sourced benzoxazines resins with healing, repair, and recycling capabilities, Prog. Org. Coat. 189 (2024), https://doi.org/10.1016/j.porgcoat.2024.108316.